

Nonadiabatic geometric quantum computation with optimal control on superconducting circuits

Jing Xu, Sai Li, Tao Chen, and Zheng-Yuan Xue*

Guangdong Provincial Key Laboratory of Quantum Engineering and Quantum Materials, and School of Physics and Telecommunication Engineering, South China Normal University, Guangzhou 510006, China

(Dated: December 22, 2024)

Quantum gates, which are the essential building blocks of quantum computers, are very fragile. Thus, to realize robust quantum gates with high fidelity is the ultimate goal of quantum manipulation. Here, we propose a nonadiabatic geometric quantum computation scheme on superconducting circuits to engineer arbitrary quantum gates, which share both the robust merit of geometric phases and the capacity to combine with the optimal control technique to further enhance the gate robustness. Specifically, in our proposal, arbitrary geometric single-qubit gates can be realized on a transmon qubit, by a resonant microwave field driving, with both the amplitude and phase of the driving being time-dependent. Meanwhile, nontrivial two-qubit geometric gates can be implemented by two capacitively coupled transmon qubits, with one of the transmon qubits' frequency being modulated to obtain effective resonant coupling between them. Therefore, our scheme provides a promising step towards fault-tolerant solid-state quantum computation.

Recently, constructing the quantum computer based on the quantum mechanical theory, is highly desired, to deal with hard problems. However, quantum systems will inevitably interact with their surrounding environment. On the other hand, the precise quantum manipulation of a quantum system is limited by the precision of controlling the driving fields. Thus, fast and robust quantum manipulation is highly desired. To construct a fault-tolerant quantum computer, topological quantum computation strategy is one of the most exciting advances [1], however, the realization of an elementary quantum gate there is still an experimental difficulty currently. Notably, geometric phases [2–4] possess the intrinsic character of noise-resilience against certain local noises, and thus can naturally be used to construct robust quantum gates for constructing a fault-tolerant quantum computer.

Previously, geometric quantum computation (GQC) has been proposed based on adiabatic evolutions with both Abelian [5] and non-Abelian geometric phases [6, 7]. However, the adiabatic evolution requires long running time such that a quantum state can be ruined by the decoherence effect. To overcome this problem, GQC with nonadiabatic evolutions has been proposed to achieve high-fidelity quantum gates based on both Abelian [8–11] with experimental demonstrations [12–16] and non-Abelian geometric phases [17, 18]. Unfortunately, the existence of systematic errors will devastate the advantage of the robustness of geometric quantum gates [19, 20]. Recently, theoretical [21, 22] and experimental works [23] have been proposed to further enhance the robustness of nonadiabatic non-Abelian geometric quantum gates against the control errors, based on three-level systems, by combining the gate operations with optimal control technique (OCT) [11, 24–26]. However, compared to the non-Abelian case, quantum gates induced from Abelian geometric phases based on two levels are easier to be realized, and the required two-qubit interaction is experimentally accessible.

Therefore, we here propose a fast GQC scheme that can be compatible with OCT on superconducting circuits, to further improve the robustness of the implemented quantum gates against control errors of the driving fields. Superconducting

circuits [27–30] have shown the unique merits of the large-scale integrability and flexibility of operations, and thus are treated as one of the promising platforms for the physical implementation of scalable quantum computation. Meanwhile, a superconducting transmon device [29] can be easily addressed to be a two-level system, i.e., the ground and first excited states $\{|0\rangle, |1\rangle\}$, which can serve as a qubit and operated by a resonant driving microwave field. Thus, arbitrary geometric single-qubit gates in our scheme can be accurately achieved after canceling the leakage to the higher excited states, mainly the second excited state $|2\rangle$, by combing with the DRAG correction [31–33]. In addition, a recent experiment [15] shows that the time-dependent effective resonant coupling can be induced in a two coupled superconducting qubits system, and thus our nontrivial geometric two-qubit control-phase gates can also be resonantly realized [34, 35] in a simple experimental setup. Furthermore, by combining with OCT, the robustness of the implemented geometric gates against the static systematic error can be greatly enhanced.

We first consider the construction of arbitrary single-qubit geometric gates in the computation basis $S_1 = \{|0\rangle, |1\rangle\}$. For a driving Hamiltonian $H_d(t)$ in the S_1 , assuming $\hbar = 1$ hereafter, its dynamic evolution is governed by the time-dependent Schrödinger equation of

$$i \frac{\partial}{\partial t} |\psi(t)\rangle = H_d(t) |\psi(t)\rangle, \quad (1)$$

where

$$|\psi(t)\rangle = e^{-i \frac{f(t)}{2}} \left[\cos \frac{\chi(t)}{2} e^{-i \frac{\beta(t)}{2}} |0\rangle + \sin \frac{\chi(t)}{2} e^{i \frac{\beta(t)}{2}} |1\rangle \right]$$

can be generally defined [25] by two time-dependent angles $\chi(t)$ and $\beta(t)$, and a parameterized phase $f(t)$. Meanwhile, the orthogonal evolution state

$$|\psi_{\perp}(t)\rangle = e^{i \frac{f(t)}{2}} \left[-\sin \frac{\chi(t)}{2} e^{-i \frac{\beta(t)}{2}} |0\rangle + \cos \frac{\chi(t)}{2} e^{i \frac{\beta(t)}{2}} |1\rangle \right]$$

of $|\psi(t)\rangle$ will also satisfy Eq. (1). By modulating the parameters of the driving field, the system undergoes a cyclic

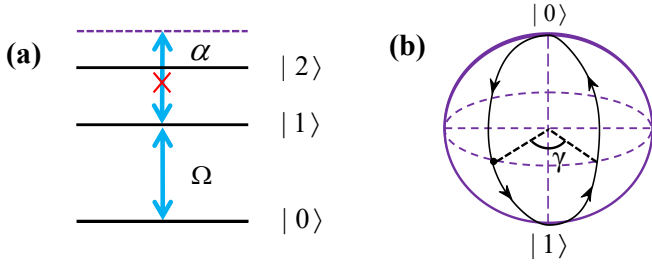


FIG. 1. Illustration of our single-qubit geometric quantum gates. (a) The qubit states are resonantly driven to realize arbitrary single-qubit gates, while the driving field will also simultaneously introduce unwanted dispersive transitions to the higher energy states. (b) Geometric illustration of the proposed single-qubit gate on a Bloch sphere.

evolution, and the initial state $|\psi(0)\rangle$ ($|\psi_{\perp}(0)\rangle$) can acquire a global phase $\gamma = [f(0) - f(\tau)]/2$ ($-\gamma$) at the final time τ , which consists of a dynamical phase of

$$\gamma_D = - \int_0^{\tau} \langle \psi(t) | H_d(t) | \psi(t) \rangle dt = \frac{1}{2} \int_0^{\tau} \frac{\dot{\beta}(t) \sin^2 \chi(t)}{\cos \chi(t)} dt,$$

and a geometric phase of

$$\gamma_G = i \int_0^{\tau} \langle \tilde{\psi}(t) | \dot{\tilde{\psi}}(t) \rangle dt = \frac{1}{2} \int_0^{\tau} \dot{\beta}(t) \cos \chi(t) dt,$$

where $|\tilde{\psi}(t)\rangle = e^{if(t)/2} |\psi(t)\rangle$. Therefore, by canceling the dynamical phase, i.e., $\gamma_D = 0$, in the global phase at the end of the cyclic evolution, we will obtain a pure geometric evolution. Since the evolution here is not governed by the adiabatic condition, the geometric phases will be induced in a faster way than that of the adiabatic schemes [4]. Especially, when the phase in Hamiltonian is a constant, our scheme will reduce to the conventional nonadiabatic schemes [10, 11]. Then, the final geometric evolution operator in S_1 is

$$U(\tau) = e^{i\gamma} |\psi(0)\rangle \langle \psi(0)| + e^{-i\gamma} |\psi_{\perp}(0)\rangle \langle \psi_{\perp}(0)| = e^{i\gamma \vec{n} \cdot \vec{\sigma}}, \quad (2)$$

where $\chi_0 = \chi(0)$, $\beta_0 = \beta(0)$. It is a rotation around the axis of $\vec{n} = (\sin \chi_0 \cos \phi_0, \sin \chi_0 \sin \phi_0, \cos \chi_0)$ by an angle 2γ , from which arbitrary single-qubit gates can be induced.

We now proceed to implement scheme on superconducting circuits. As shown in Fig. 1(a), the two lowest levels $|0\rangle$ and $|1\rangle$ of a single transmon qubit can be resonantly coupled by a microwave field with time-dependent amplitude $\Omega(t)$ and phase $\phi(t)$. Into the interaction picture, neglecting the high-order oscillating terms by the rotating-wave approximation. Then, the Hamiltonian of the system in S_1 is

$$H_d(t) = \frac{1}{2} \begin{pmatrix} 0 & \Omega(t)e^{i\phi(t)} \\ \Omega(t)e^{-i\phi(t)} & 0 \end{pmatrix}. \quad (3)$$

In the following, to let $H_d(t)$ fulfil Eq. (1) at any moment, we obtain the relation of the parameters as

$$\dot{f}(t) = -\frac{\dot{\beta}(t)}{\cos \chi(t)}, \quad (4a)$$

$$\dot{\chi}(t) = -\Omega(t) \sin[\beta(t) + \phi(t)], \quad (4b)$$

$$\dot{\beta}(t) = -\Omega(t) \cot \chi(t) \cos[\beta(t) + \phi(t)]. \quad (4c)$$

Thus, we find that a target evolution path of the evolution state $|\psi(t)\rangle$ ($|\psi_{\perp}(t)\rangle$) can be determined by designing the parameters $\Omega(t)$ and $\phi(t)$ of the microwave field. Here, we construct a single-loop evolution path by defining the evolution parameters $\chi(t)$ and $\beta(t)$ to fulfill a cyclic evolution, as illustrated in Fig. 1(b). Thus we can inversely determine the parameters $\Omega(t)$ and $\phi(t)$, i.e.,

$$\Omega(t) = -\frac{\dot{\chi}(t)}{\sin(\beta(t) + \phi(t))}, \quad (5)$$

$$\phi(t) = \arctan\left(\frac{\dot{\chi}(t)}{\dot{\beta}(t)} \cot \chi(t)\right) - \beta(t).$$

In addition, we also need to ensure the accumulated dynamical phases are zero at the end of cyclic evolution to achieve pure geometric operations.

Specifically, we consider rotations around X and Z axes as two typical examples in detail. Firstly, to realize the geometric rotation operators around the X axis, we divide a single-loop evolution path into four equal parts, which aims to cancel dynamical phases at the end of cyclic evolution. The shape of $\chi_j(t)$ and initial values of $\beta_j(t)$ in each part are

$$\begin{aligned} t \in [0, \tau/4] : & \quad \chi_1(t) = \pi[1 + \sin^2(2\pi t/\tau)]/2, \\ & \quad \beta_1(0) = 0, \\ t \in [\tau/4, \tau/2] : & \quad \chi_2(t) = \pi[1 + \sin^2(2\pi t/\tau)]/2, \\ & \quad \beta_2(\tau/4) = \beta_1(\tau/4) - \gamma, \\ t \in [\tau/2, 3\tau/4] : & \quad \chi_3(t) = \pi[1 - \sin^2(2\pi t/\tau)]/2, \\ & \quad \beta_3(\tau/2) = \beta_2(\tau/2), \\ t \in [3\tau/4, \tau] : & \quad \chi_4(t) = \pi[1 - \sin^2(2\pi t/\tau)]/2, \\ & \quad \beta_4(3\tau/4) = \beta_3(3\tau/4) + \gamma, \end{aligned} \quad (6)$$

where the shape of $\beta_j(t)$ is set as $\beta_j(t) = -\int f_j(t) \cos \chi_j(t) dt$ for the j th part with $f_j(t) = \cos 2\chi_j(t)/5$. Therefore, we can obtain the shape of $\Omega(t)$ and $\phi(t)$ in the different evolution parts according to Eq. (5). Meanwhile, in this setting, the dynamical phase is zero and the geometric phase is $\gamma_G = \gamma$ due to the saltation of $\beta(t)$ at the moment of $t = \tau/4$ and $t = 3\tau/4$. In this way, the geometric rotation operations $e^{i\gamma \sigma_x}$ can be realized.

Similarly, to realize the geometric rotation operators around the Z axis, we divide a single-loop evolution path into only two equal parts. The shape of $\chi_j(t)$ and initial values of $\beta_j(t)$ in the each parts are

$$\begin{aligned} t \in [0, \tau/2] : & \quad \chi_1(t) = \pi \sin^2(\pi t/\tau), \\ & \quad \beta_1(0) = 0, \\ t \in [\tau/2, \tau] : & \quad \chi_2(t) = \pi \sin^2(\pi t/\tau), \\ & \quad \beta_2(\tau/2) = \beta_1(\tau/2) - \gamma, \end{aligned} \quad (7)$$

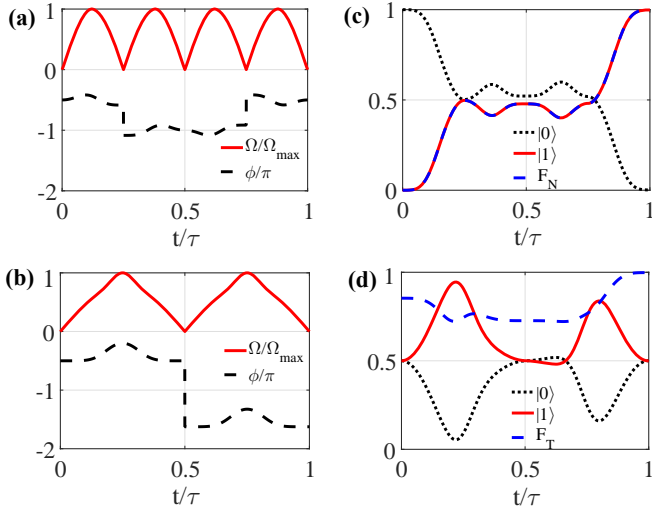


FIG. 2. Implementation of single-qubit geometric gates and their performance. The shapes of $\Omega(t)$ and $\phi(t)$ for the NOT and Phase gates are shown in (a) and (b), respectively. The qubit-state population and the state-fidelity dynamics of the NOT and Phase gate operations are shown in (c) and (d), respectively.

where the shape of $\beta_j(t)$ is set to be $\beta_j(t) = -\int \dot{f}_j(t) \cos \chi_j(t) dt$ for the j th part with $f_j(t) = [2\chi_j(t) - \sin 2\chi_j(t)]/5$. The shape of $\Omega(t)$ and $\phi(t)$ can also be obtained in the different evolution parts according to Eq. (5). By only the saltation of $\beta(t)$ at the moment of $t = \tau/2$, the dynamical phase at the end of the cyclic evolution can be eliminated and the pure geometric phase can be accumulated. Therefore, the geometric rotations $e^{i\gamma\sigma_z}$ can be realized.

Due to the weak anharmonicity of the transmon qubit, here, the DRAG correction [31–33] is also introduced to suppress the leakage error beyond the qubit basis. Considering all effects of decoherence and dominant counter-rotating terms, we use the Lindblad master equation

$$\dot{\rho}_1 = i[\rho_1, H_d(t) + H_{\text{leak}}(t)] + [\Gamma_1 \mathcal{L}(\sigma_1) + \Gamma_2 \mathcal{L}(\sigma_2)], \quad (8)$$

with

$$H_{\text{leak}}(t) = -\alpha|2\rangle\langle 2| + \left[\sqrt{2}\Omega(t)e^{i\phi(t)}|1\rangle\langle 2| + \text{H.c.} \right], \quad (9)$$

to evaluate the performance of the implemented single-qubit gates, where ρ_1 is the density matrix of the considered system and $\mathcal{L}(\mathcal{A}) = \mathcal{A}\rho_1\mathcal{A}^\dagger - \mathcal{A}^\dagger\mathcal{A}\rho_1/2 - \rho_1\mathcal{A}^\dagger\mathcal{A}/2$ is the Lindbladian of the operator \mathcal{A} with $\sigma_1 = |0\rangle\langle 1| + \sqrt{2}|1\rangle\langle 2|$ and $\sigma_2 = |1\rangle\langle 1| + 2|2\rangle\langle 2|$, and Γ_1 and Γ_2 are the decay and dephasing rates of the transmon qubit, respectively. We consider the case of $\Gamma_1 = \Gamma_2 = \Gamma = 2\pi \times 2$ kHz, which is easily accessible with current experimental technologies. The anharmonicity of the transmon is set to be $\alpha = 2\pi \times 300$ MHz, and the maximum amplitude $\Omega_{\text{max}} = 2\pi \times 16$ MHz. We next take the NOT (N) and Phase (T) gates as two typical examples, which can be realized by setting $\chi_1(0) = \pi/2$, $\gamma = \pi/2$ and $\chi_1(0) = 0$, $\gamma = -\pi/8$ with the same $\beta_1(0) = 0$, respectively. Assuming the maximum amplitude $\Omega_{\text{max}} = 2\pi \times 16$ MHz, the

cyclic evolution time τ is about 102 ns for the NOT gate and 125 ns for the Phase gate. The corresponding shapes of $\Omega(t)$ and $\phi(t)$ for the NOT and Phase gates are shown in Figs. 2(a) and 2(b), respectively. Assuming the initial states of quantum system are $|\Phi(0)\rangle_N = |0\rangle$ and $|\Phi(0)\rangle_T = (|0\rangle + |1\rangle)/\sqrt{2}$ for the cases of the NOT and Phase gates, the obtained fidelities are as high as $F_N = 99.87\%$ and $F_T = 99.80\%$, as shown in Figs. 2(c) and 2(d), respectively. In addition, we find the gate fidelities of can reach $F_N^G = 99.87\%$ and $F_T^G = 99.84\%$, respectively.

Here, we proceed to design the evolution path by combining it with OCT [24–26], to further enhance the robustness of our scheme against systematic error. Specifically, in the case of the geometric Z rotations, we consider the existence of the static systematic error, i.e. $\Omega(t) \rightarrow (1 + \epsilon)\Omega(t)$. Then, the Hamiltonian will be

$$H_\epsilon(t) = (1 + \epsilon)\frac{\Omega(t)}{2}e^{i\phi(t)}|0\rangle\langle 1| + \text{H.c.} \quad (10)$$

Due to the symmetry of the evolution path of the considered geometric rotations, we take the first path $[0, \tau/2]$ to evaluate the gate robustness, which can be calculated by the perturbation theory with probability amplitude P defined as

$$P = |\langle \psi(\tau/2) | \psi_\epsilon(\tau/2) \rangle|^2 = 1 + \tilde{O}_1 + \tilde{O}_2 + \dots, \quad (11)$$

where $|\psi_\epsilon(\tau/2)\rangle$ is the state with the systematic error, and \tilde{O}_n denotes the term of the perturbation at the n th order. Up to the second order, it is calculated to be

$$\tilde{O}_1 = 0, \quad \tilde{O}_2 = -\epsilon^2 \left| \int_{\chi_0}^{\chi_{\tau/2}} e^{-if} \sin^2 \chi d\chi \right|^2. \quad (12)$$

Defining $f(\chi) = \eta[2\chi - \sin(2\chi)]$, $\beta_1(0) = 0$ and $\beta_2(\tau/2) = \beta_1(\tau/2) - \gamma$, resulting in $\tilde{O}_2 = -\epsilon^2 \sin^2 \eta\pi/(2\eta)^2$, we can ensure $\tilde{O}_2 = 0$ for $P_2 = 1$ by setting η to a non-zero integer, which directly demonstrates that the designed evolution path is combined with OCT. It is important to note that when $\eta = 0$, $\tilde{O}_2 = -\pi^2\epsilon^2/4$, the current implementation will reduce to the previous non-adiabatic schemes [8–11].

For a typical example, we simulate the Phase gate under the effect of the systematic error $\epsilon\Omega_{\text{max}}$ in the range of $2\pi \times [-5, 5]$ MHz with $\Omega_{\text{max}} = 2\pi \times 16$ MHz. In Fig. 3(a), we plot the gate fidelity as a function of the systematic error $\epsilon\Omega_{\text{max}}$ for the cases of $\eta = 0$ and $\eta = 1$ without decoherence with the gate time τ being 405 ns and 98 ns, respectively. We find that the robustness of our geometric gates in the case of $\eta = 1$ can be significant improved comparing with the case of $\eta = 0$ (previous implementations). Meanwhile, as shown in Figs. 3(b) and 3(c), considering both the systematic error and the decoherence effects, our implementation still has the advantage of improving robustness in a certain decoherence range.

We now turn to the implementation of nontrivial two-qubit geometric gates based on two capacitively coupled transmons [36–38], which are respectively labeled by transmons A and B with qubit frequency $\omega_{A,B}$ and anharmonicity $\alpha_{A,B}$. However, the frequency difference $\Delta = \omega_A - \omega_B$ and coupling

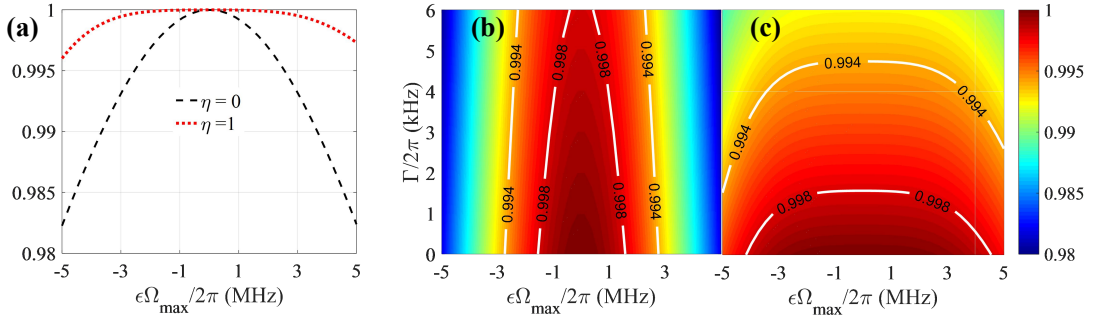


FIG. 3. Single-qubit gate performance without ($\eta = 0$) and with ($\eta = 1$) optimization. (a) The gate fidelity of the Phase gate with different η under the systematic error ϵ without decoherence. The gate fidelity of the Phase gate without and with optimization are shown in (b) and (c), respectively, under both the systematic error $\epsilon\Omega_{\max}$ and a uniform decoherence rate Γ .

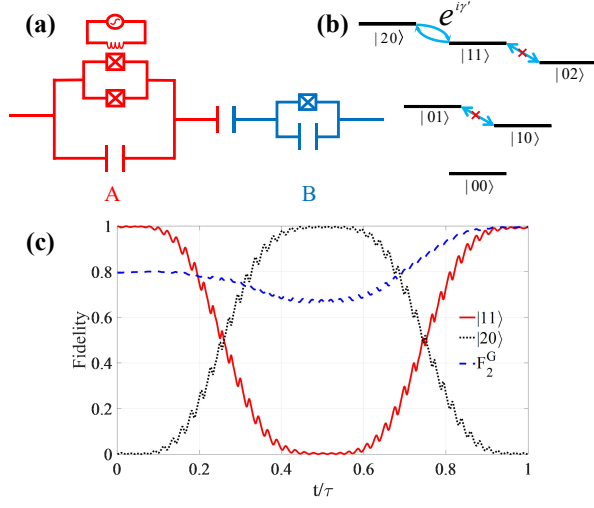


FIG. 4. Illustration of the implementation of the two-qubit geometric gates. (a) Two capacitively coupled transmon qubits configuration for non-trivial two-qubit gates, where the frequency of qubit A is ac modulated to induce effective resonant interaction between the two qubits. (b) The coupling structure for the states of the two transmon qubits. (c) The gate fidelity of a nontrivial geometric control-phase gate with $\gamma' = \pi/2$.

strength g between this two transmons A and B are usually fixed and can not be adjustable. Profitably, in a recent experimental setup [15], as illustrated in in Fig. 4(a), time-dependent tunable coupling interaction can be realized by introducing a qubit-frequency driving $\zeta(\epsilon(t))$ on transmon A, which can be experimentally induced by adding a longitudinal field $\epsilon(t) = \zeta^{-1}(\dot{\mathcal{F}}(t))$, where $\mathcal{F}(t) = \lambda(t) \sin[\nu t + \varphi(t)]$ with ν and $\varphi(t)$ being the frequency and phase of the longitudinal field, respectively. Then, in the interaction picture, the effective Hamiltonian is

$$H_t(t) = g[|10\rangle_{AB}\langle 01|e^{i\Delta t} + \sqrt{2}|11\rangle_{AB}\langle 02|e^{i(\Delta+\alpha_B)t} + \sqrt{2}|20\rangle_{AB}\langle 11|e^{i(\Delta-\alpha_A)t}]e^{-i\lambda(t)\sin[\nu t + \varphi(t)]} + \text{H.c.} \quad (13)$$

The corresponding coupling configuration of these two coupled transmons is shown in Fig. 4(b). We consider the case

of the resonant interaction in the subspace $\{|11\rangle_{AB}, |20\rangle_{AB}\}$ by choosing the driving frequency $\nu = \Delta - \alpha_A$ with $g \ll \{\nu, \Delta - \nu, \Delta + \alpha_B - \nu\}$, and then using Jacobi-Anger identity and neglecting the high-order oscillating terms, the obtained effective Hamiltonian can be reduced to

$$H_2(t) = \frac{1}{2} \begin{pmatrix} 0 & g'(t)e^{i\varphi(t)} \\ g'(t)e^{-i\varphi(t)} & 0 \end{pmatrix}, \quad (14)$$

in the two-qubit subspace $\{|11\rangle_{AB}, |20\rangle_{AB}\}$, where $g'(t) = 2\sqrt{2}gJ_1(\lambda(t))$ is effective time-dependent coupling strength between transmon qubits A and B, with $J_1(\lambda(t))$ being the Bessel function of the first kind. Similar to the single-qubit case in Eq. (3), within the two-qubit subspace $\{|00\rangle_{AB}, |01\rangle_{AB}, |10\rangle_{AB}, |11\rangle_{AB}\}$, we can also use the effective Hamiltonian $H_2(t)$ to acquire a pure geometric phase $e^{i\gamma'}$ condition on two-qubit state of $|11\rangle_{AB}$ by a cyclic evolution. The resulting geometric control-phase gates is

$$U_2(\gamma') = \text{diag}(1, 1, 1, \exp(i\gamma')). \quad (15)$$

Here, we also use the Lindblad master equation to evaluate the nontrivial two-qubit geometric control-phase gates with $\gamma' = \pi/2$ as a typical example. We set the parameters of the transmon qubits as $\Delta = 2\pi \times 500$ MHz, $\alpha_A = 2\pi \times 320$ MHz, $\alpha_B = 2\pi \times 300$ MHz and $g = 2\pi \times 5$ MHz, and the driving frequency $\nu = \Delta - \alpha_A = 2\pi \times 180$ MHz. Furthermore, we fix the evolution time τ' for the two-qubit gate to be 250 ns under a corresponding coupling strength of $g'_{\max} = 2\pi \times 8$ MHz, and the form of the auxiliary parameters $\chi(t)$, $\beta(t)$ being the same as that of the single-qubit case for the geometric rotation operators around Z axis. In this way, the shape of $g'(t)$ and $\varphi(t)$ can finally be determined. In addition, we can numerically define $\lambda(t)/\nu = J_1^{-1}[g'(t)/(2\sqrt{2}g)]$, and then use the original Hamiltonian $\mathcal{H}_t(t)$ to faithfully verify our proposal. As shown in Fig. 4(c), we can get the gate fidelity $F_2^G = 99.53\%$. Finally, comparing the two-qubit Hamiltonian $H_2(t)$ with the single-qubit Hamiltonian $H_d(t)$, one find that they are in the same form, both with the tunable coupling strength and phase. Thus, the OCT presented in the single-qubit case can be directly incorporated in the two-qubit case.

In summary, we have proposed a general method to construct fast universal GQC. Then, we physically implement our proposal on superconducting circuits, where arbitrary single-qubit gates are realized by resonant driving on a transmon qubit with a microwave field, and nontrivial two-qubit gates can be implemented by ac driving on one of the transmon qubits, which leads to effectively resonant coupling between them. Finally, our scheme can combine with OCT to further enhance the gate robustness against the static systematic error. We note that our proposal can be expanded to a two-dimensional capacitively coupled lattice of transmon qubits, and thus provides a promising step towards fault-tolerant quantum computation on superconducting circuits.

This work was supported by the National Natural Science Foundation of China (Grant No. 11874156).

* zyxue83@163.com

- [1] C. Nayak, S. H. Simon, A. Stern, M. Freedman, S. D. Sarma, *Rev. Mod. Phys.* **80**, 1083 (2008).
- [2] M. V. Berry, *Proc. R. Soc. Lond., Ser. A* **392**, 45 (1984).
- [3] F. Wilczek and A. Zee, *Phys. Rev. Lett.* **52**, 2111 (1984).
- [4] Y. Aharonov and J. Anandan, *Phys. Rev. Lett.* **58**, 1593 (1987).
- [5] J. A. Jones, V. Vedral, A. Ekert, and G. Castagnoli, *Nature (London)* **403**, 869 (2000).
- [6] P. Zanardi and M. Rasetti, *Phys. Lett. A* **264**, 94 (1999).
- [7] L. M. Duan, J. I. Cirac, and P. Zoller, *Science* **292**, 1695 (2001).
- [8] X. B. Wang and M. Keiji, *Phys. Rev. Lett.* **87**, 097901 (2001).
- [9] S. L. Zhu and Z. D. Wang, *Phys. Rev. Lett.* **89**, 097902 (2002).
- [10] P. Z. Zhao, X. D. Cui, G. F. Xu, E. Sjöqvist, and D. M. Tong, *Phys. Rev. A* **96**, 052316 (2017).
- [11] T. Chen and Z.-Y. Xue, *Phys. Rev. Appl.* **10**, 054051 (2018).
- [12] G. Falci, R. Fazio, G. M. Palma, J. Siewert, and V. Vedral, *Nature (London)* **407**, 355 (2000).
- [13] D. Leibfried *et al.*, *Nature (London)* **422**, 412 (2003).
- [14] J. Du, P. Zou, and Z. D. Wang, *Phys. Rev. A* **74**, 020302(R) (2006).
- [15] J. Chu *et al.*, arXiv:1906.02992.
- [16] Y. Xu *et al.*, arXiv:1910.12271.
- [17] E. Sjöqvist, D. M. Tong, L. Mauritz Andersson, B. Hessmo, M. Johansson, and K. Singh, *New J. Phys.* **14**, 103035 (2012).
- [18] G. F. Xu, J. Zhang, D. M. Tong, E. Sjöqvist, and L. C. Kwek, *Phys. Rev. Lett.* **109**, 170501 (2012).
- [19] S. B. Zheng, C. P. Yang, and F. Nori, *Phys. Rev. A* **93**, 032313 (2016).
- [20] J. Jing, C.-H. Lam, and L.-A. Wu, *Phys. Rev. A* **95**, 012334 (2017).
- [21] B.-J. Liu, X.-K. Song, Z.-Y. Xue, X. Wang, and M.-H. Yung, *Phys. Rev. Lett.* **123**, 100501 (2019).
- [22] S. Li, T. Chen, and Z.-Y. Xue, *Adv. Quantum Technol.* **3**, 2000001 (2020).
- [23] T. Yan *et al.*, *Phys. Rev. Lett.* **122**, 080501 (2019).
- [24] A. Ruschhaupt, X. Chen, D. Alonso, and J. G. Muga, *New J. Phys.* **14**, 093040 (2012).
- [25] D. Daems, A. Ruschhaupt, D. Sugny and S. Guérin, *Phys. Rev. Lett.* **111**, 050404 (2013).
- [26] S. J. Glaser *et al.*, *Eur. Phys. J. D* **69**, 279 (2015).
- [27] J. Clarke and F. K. Wilhelm, *Nature* **453**, 1031 (2008).
- [28] J. Q. You and F. Nori, *Nature* **474**, 589 (2011).
- [29] M. H. Devoret and R. J. Schoelkopf, *Science* **339**, 1169 (2013).
- [30] G. Wendin, *Rep. Prog. Phys.* **80**, 106001 (2017).
- [31] J. M. Gambetta, F. Motzoi, S. T. Merkel, and F. K. Wilhelm, *Phys. Rev. A* **83**, 012308 (2011).
- [32] T. H. Wang, Z. X. Zhang, L. Xiang, Z. H. Gong, J. L. Wu, and Y. Yin, *Sci. China: Phys. Mech. Astro.* **61**, 047411 (2018).
- [33] T. H. Wang *et al.*, *New J. Phys.* **20**, 065003 (2018).
- [34] F. W. Strauch, P. R. Johnson, A. J. Dragt, C. J. Lobb, J. R. Anderson, and F. C. Wellstood, *Phys. Rev. Lett.* **91**, 167005 (2003).
- [35] L. DiCarlo *et al.*, *Nature* **467**, 574 (2010).
- [36] M. Reagor *et al.*, *Sci. Adv.* **4**, eaao3603 (2018).
- [37] S. A. Caldwell *et al.*, *Phys. Rev. Appl.* **10**, 034050 (2018).
- [38] X. Li *et al.*, *Phys. Rev. Appl.* **10**, 054009 (2018).